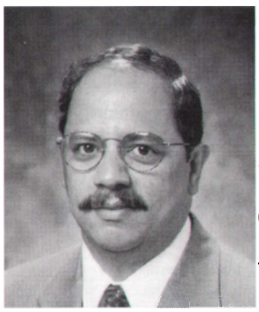

Sudhakar Rao
Northrop Grumman Aerospace Systems
One Spacepark
Redondo Beach, CA 90278 USA
Tel: +1 (310) 813-5405
E-mail: sudhakar.rao@ngc.com

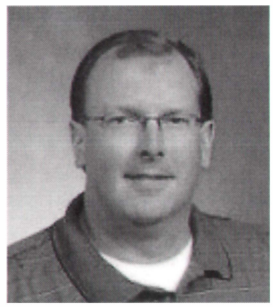

Jay Kralovec
2507 Canterbury Circle
Viera, FL 32955 USA
Tel: +1 (321) 631-7240
E-mail: jay.kralovec@ieee.org

Introduction

This paper is a joint collaborative effort from the Universidad Complutense de Madrid, Spain, and the Jet Propulsion Laboratory, Pasadena, USA. The authors, Nuria Llombart, Robert Dengler, and Ken Cooper, describe a novel reflector system that can rapidly scan a terahertz beam for a high-resolution standoff-imaging radar application, without compromising the beam quality. The design and measured results for a Gregorian confocal-reflector antenna, using a flat rotating mirror for beam scanning at 675 GHz, are presented.

Terahertz Antenna System for a Near-Video-Rate Radar Imager

Nuria Llombart[1], Robert J. Dengler[2], and Ken B. Cooper[2]

[1]Optics Department
Universidad Complutense de Madrid, Spain
E-mail: nuria.llombart@opt.ucm.es

[2]Jet Propulsion Laboratory, California Institute of Technology
Pasadena, USA
E-mail: no6b@no6b.jpl.nasa.gov, ken.b.cooper@jpl.nasa.gov

Abstract

In this contribution, we present simulations and measurements of a reflector system that can rapidly scan a terahertz beam for a high-resolution standoff-imaging application, without compromising the beam quality. The antenna system utilizes a Gregorian confocal-reflector geometry, with a small mechanical rotating mirror. The system has been successfully fabricated and tested, with THz imagery of targets at a 25 m standoff range being obtained In five seconds, for the current configuration. We also describe how frame rates exceeding 2 Hz can be achieved using a heterodyne array of just a few elements, with or without a multiplexing technique.

Keywords: Submillimeter wave antennas; multireflector antennas; scanning antennas; submillimeter wave imaging; radar imaging

1. Introduction

The detection of weapons or contraband concealed on persons has been demonstrated with active and passive millimeter- and sub-millimeter-wave imagers [1-7]. Several commercial systems now exist for through-clothes imaging at few-meter standoff distances in the frequency range of 100-300 GHz [3]. For situations that call for more-remote imaging – for example, at distances greater than 20 m, where a diffraction-limited beamwidth of less than one milliradian is desirable – concealed-weapons detection using mm and sub-mm radiation becomes significantly more difficult. This is because of the tradeoff between diffractive resolution loss at lower frequencies, and signal attenuation from both the atmosphere and clothing as frequencies approach 1 THz. As a compromise involving these tradeoffs, we have developed a THz imaging system operating at 675 GHz. This was high enough to ensure good image resolution for an aperture diameter no larger than 1 m and at standoff ranges up to about 30 m. To overcome signal attenuation, we also relied on an active, heterodyne transceiver architecture, which currently achieves about –6 dBm of output power. In addition, the JPL THz imaging system utilized the frequency-modulated continuous-wave (FMCW) radar technique to generate three-dimensional target images. This was critical for reducing scene clutter and interference from specular reflections [5-7].

Several of the THz imaging radar's subsystems stand in contrast to conventional radars. These include the low-noise microwave chirp generator, capable of sweeping between 1.8 and 3.2 GHz (prior to multiplication by 18) in less than 1 ms [8]. Another example is the THz source chain utilizing Schottky-diode frequency multipliers (a technology originally developed for astrophysics and Earth-science applications), and custom image processing algorithms to "peel away" clothing layers from the radar's target. However, no less important to the radar's successful operation was its antenna design and performance, which is the subject of this article.

The first-generation THz radar [5] had a simple reflector system that focused a 570-600 GHz beam to a sub-centimeter spot size at a 4 m standoff range, using a 40 cm-diameter ellipsoidal antenna. A scene image was acquired by slowly rotating the entire ~50 kg radar platform in azimuth and elevation. This naturally required very long imaging times, on the order of minutes. While this system provided a proof-of-principle for long-range concealed-objects detection, it clearly needed improvement in both standoff range and, especially, imaging speed.

A second-generation THz imaging radar was thus developed to generate images in a few seconds rather than a few minutes, and at a six-times-longer standoff range of 25 m. Although still not fast enough for most real-life threat-detection applications, the overall system design could be readily scaled to higher speeds, possibly even reaching near-video frame rates (5-10 Hz) using a few-element transceiver array. These much-higher imaging speeds were primarily enabled by a new antenna design of the THz radar, which was described, including simulations, in [9]. The design consisted of a multi-reflector geometry, optimized to achieve fast beam steering without compromising beam quality. The beam steering was achieved by rotating a small (13 cm), flat secondary mirror, while the main 100 cm ellipsoidal antenna remained stationary. This design has now been fabricated and assembled (see Figure 1). A description of the new design's test results is presented in Section 2. This is followed by a presentation of a concept for achieving another order-of-magnitude improvement of the imaging time by scanning a heterodyne beam array, possibly in conjunction with a novel time-delay multiplexing technique [10].

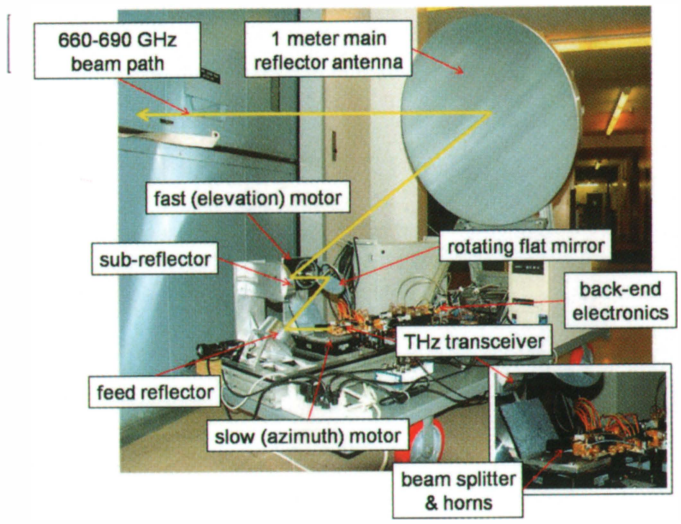

Figure 1. A fast-scanning, long-range THz imaging radar. The 1 m diameter ellipsoidal main reflector permits cm-scale cross-range resolution at 25 m standoff ranges. A small rotating mirror rapidly steers the projected beam over a 50 × 50 cm target down range. The 660-690 GHz beam is chirped in an FMCW mode for sub-cm range resolution.

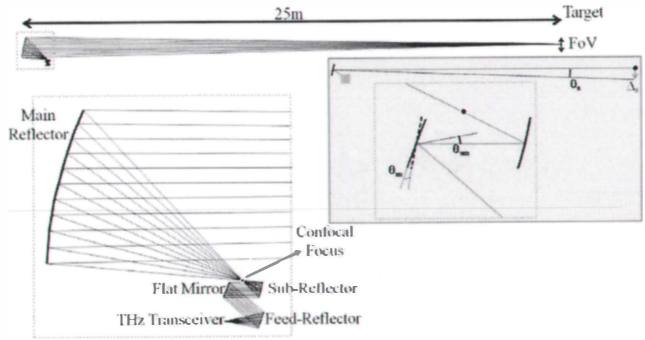

Figure 2. A ray-tracing picture in the vertical plane of the antenna system at the nominal rotating-mirror position. The figure in the inset shows the angles that describe the mirror rotation (θ_m) and beam scanning (θ_{sm} and θ_m).

2. Antenna System

2.1 Description

The proposed antenna system utilizes a confocal Gregorian dual-reflector system, illuminated by a collimated beam, generated by a parabolic reflector. The collimated beam is steered by a mechanically rotating flat mirror (see Figure 2). Such a configuration exhibits excellent scanning performance [9-11]. For operation at sub-millimeter wavelengths and standoff ranges of many meters, the imaging targets are electrically very close to the antenna's aperture. The main reflector surface must therefore be an ellipse, instead of a parabola, in order to achieve the best imaging performance. The imaging radar's antenna system was fabricated with essentially the same geometry proposed in [9], and its main specifications are described in Table 1.

Figure 2 shows a ray-tracing picture of the antenna system for the nominal angular position (θ_m) of the rotation mirror (i.e.,

Table 1. The antenna system specifications.

Specification	Quantity
Frequency of operation	660-690 GHz
Rx/Tx polarization	Linear (horizontal)
Main antenna aperture	1 m
Simulated Δ_p (beamwidth at 25 m)	1.3 cm (0.03°)
Stand-off range	25 m
Field of view (FoV)	0.5 m × 0.5 m (1.1° × 1.1°)
System magnification (M)	10
Maximum mirror rotation angle	$\theta_m = \pm 3°$

scanning towards the center of the field of view). The system consists of the following components:

- The surface of the *main reflector antenna* is an ellipsoid, with one near focus at the confocal point and the other 25 m down range from the antenna aperture, as shown in Figure 2. The main reflector's diameter (1 m) is not oversized to achieve the beam steering, and therefore the half-power width of the focused beam at 25 m (see Table 1) is basically the same over the whole field of view. For simplicity, we will refer to such width as the HPBW for the rest of the paper.

- The *sub-reflector* is a parabolic reflector that focuses a collimated beam to the same confocal point as the main antenna. The ratio of the sub-reflector's focal distance to the main-reflector's near focal distance determines the system magnification. This was chosen to be $M = 10$. The diameter of the sub-reflector needed to be oversized from the 10 cm needed for the nominal beam, to 14 cm, in order to maintain the spillover losses and keep the beamwidth constant over the field of view.

- The sub-reflector is illuminated by a collimated beam coming from a *flat mirror*, 13 cm in diameter, which rotates through an angle θ_m about two axes (elevation and azimuth): see the corresponding elevation and azimuth motors in Figure 1. This rotation allows steering the collimated beam by $\theta_{sm} = 2\theta_m$. Because of the confocal geometry, the beam is then focused by the main antenna, and steered towards $\theta_s = \theta_{sm}/M/BDF$, where M is the system magnification and BDF is the beam-deviation factor [12].

- The *flat mirror* is tilted on two axes (see θ_m in the inset in Figure 2) with respect to its center, one for elevation and one for azimuth.

- In order to generate a collimated beam onto the flat mirror, a parabolic *feed reflector* is used. The feed reflector does not have any impact on the beam-scanning mechanism.

- A *beam splitter* is used in the THz transceiver to accomplish transmitter/receiver (Tx/Rx) duplexing. It consists of a thin silicon wafer oriented at 45° from the outgoing beam. It combines and divides the transmitted and received signals with extremely high isolation, at the cost of a 6 dB two-way signal loss from its unused port. A circulator, which would eliminate this loss, cannot be easily obtained at 670 GHz. However, progress in low-loss quasi-optical Faraday rotators may eventually make THz circulators feasible [13].

- Finally, two *diagonal horns*, one for the transmitted beam and the other for the received beam, are placed at the focus of the feed reflector on either side of the beam splitter. The horns, manufactured by Virginia Diodes, are based in the design in [14], and have 25 dBi directivity and a 10 dB-taper angle of 11.6°.

This antenna geometry was selected because it presents significant benefits for fast beam-scanning applications. From the mechanical point of view, the main aperture remains stationary, and only the small flat mirror is rotated. This is in contrast to the first-generation THz radar imager, where the 40 cm main aperture was rotated along with the system's front-end electronics. With a diameter of 13 cm, the flat rotating mirror can have a small inertia for a rapid nodding motion. In addition, all of the radar's electronic components remain stationary in the current design, reducing possible spurious phase shifts coming from flexing coaxial cable or waveguides. Finally, from the antenna point of view, steering the beam when it is collimated into an envelope of parallel rays – rather than when it is diverging toward the main reflector – results in negligible aberrations over the large field of view, typically 40-45 half-power beamwidths (HPBWs).

2.2 Fabrication

The most-critical antenna component to be fabricated was the 1 meter-diameter ellipsoid. For the current prototype, CNC milling of aluminum was performed by Custom Microwave Inc. to achieve a targeted local-surface roughness (rms) of less than 25 μm, and an overall curvature accuracy better than 75 μm. However, no direct surface profiles have been made to confirm that these specifications were achieved. An rms of 20 μm implies an antenna-gain loss of approximately 1.3 dB, resulting in a 2.6 dB two-way SNR reduction [15]. A diamond-turned fabrication process would provide a more accurate surface for less gain loss or for operation at higher frequencies, but diamond cutting such a large off-axis reflector is impractical. The feed- and sub-reflectors, which have significantly smaller diameters, were made from diamond-turned aluminum. A small effort was made to reduce the weight of the antenna by thinning its back side and adding ribbing for stiffness, resulting in a final weight of about 52 lbs. We expect that this weight can be reduced by about a factor of two following additional design work.

Another critical antenna component was the fast-steering flat mirror, which is tilted about two orthogonal axes (elevation and azimuth) using a pair of Newport Corp. precision rotation stages. For the fast elevation scanning, the RGV100BL rotary stage achieves accelerations up to about 20,000°/s^2, while maintaining accuracies much better than the required 0.05°. This fast acceleration is one of the keys to achieving short imaging times, as described in Section 3.

The platform to hold the entire antenna system was designed using a combination of off-the-shelf aluminum framing and custom aluminum support plates. The feed- and sub-reflectors were secured with respect to each other using steel pins, while the rotating flat mirror, the main aperture, and the transmitting and receiving horns were fixed with screws but no pins. After mounting the various antenna elements, small hand adjustments of approximately 1° were made to the tilt of the feed- and sub-reflec-

tor assemblies until good scanning-beam patterns were achieved. This manual alignment was likely necessary to compensate for an inaccurate placement of the heavy main aperture. Even better alignment can likely be realized by using a coordinate measuring machine (CMM), but that has not been pursued so far.

2.3 Measurements and Simulations

Calibrated antenna measurements in anechoic chambers, very common at lower frequencies, are difficult and expensive to achieve at 650 GHz. In order to experimentally assess the scanning THz antenna system's performance, an image of a 25 m-distant grid of 3 mm-diameter gold beads, suspended in a wooden frame using 100 μm diameter nylon threads, was therefore acquired with

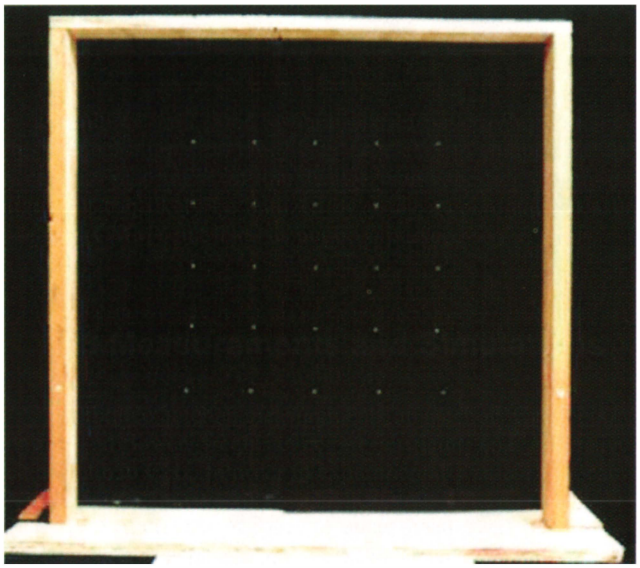

Figure 3a. Antenna pattern assessment: The calibration target consisted of a 5 × 5 grid of 3 mm diameter gold beads, suspended by thin nylon thread, and spanning 50 × 50 cm.

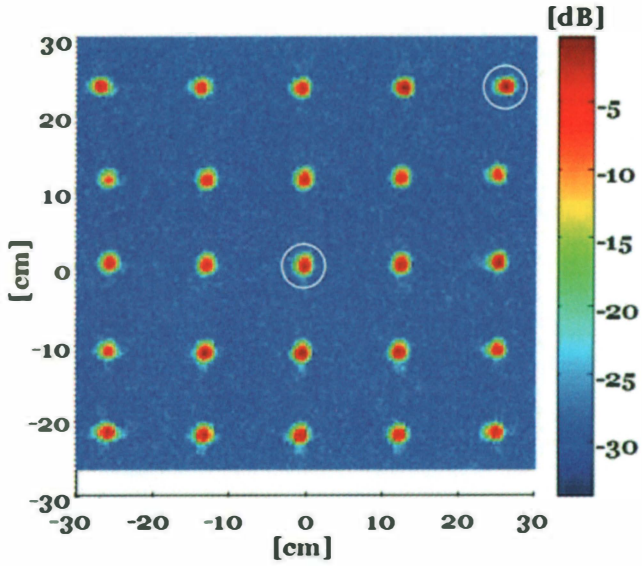

Figure 3b. Antenna pattern assessment: A reflected radar power image of the bead grid, revealing good beam shapes over the entire field of view. The outlined beads are analyzed in Figure 4.

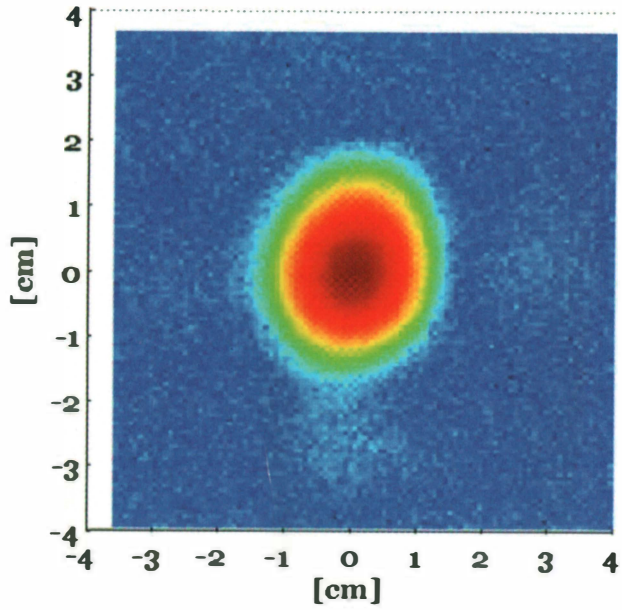

Figure 4a. A fine scan of the measured center bead, showing a nearly circular beam pattern. The same color/power scale as in Figure 3b is used here. The integration time was 0.44 ms per pixel.

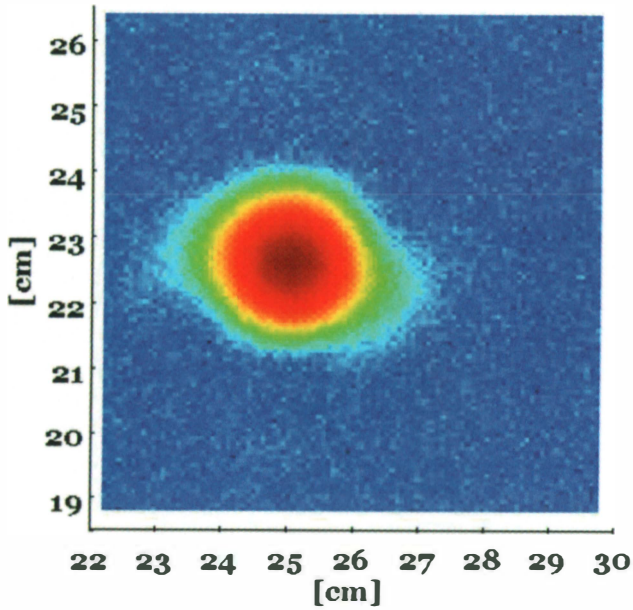

Figure 4b. A fine scan of the measured upper-right bead, showing a nearly circular beam pattern. The same color/power scale as in Figure 3b is used here. The integration time was 0.44 ms per pixel.

the radar system. The same method was used to characterize the first prototype in [5]. The bead spacing was 12.5 cm, so that the entire grid covered a 50 × 50 cm square, which corresponded to the system's designed field of view. Figure 3a shows a photograph of the target, and Figure 3b shows the radar power reflected from the grid of beads, integrated over a range swath of about 4 cm, centered at the beads. A closer analysis of the center and upper-right beads pattern is shown in Figure 4. With such an image, the beam-pattern shape over several steering directions could be characterized simultaneously, which was useful for aligning the antenna system.

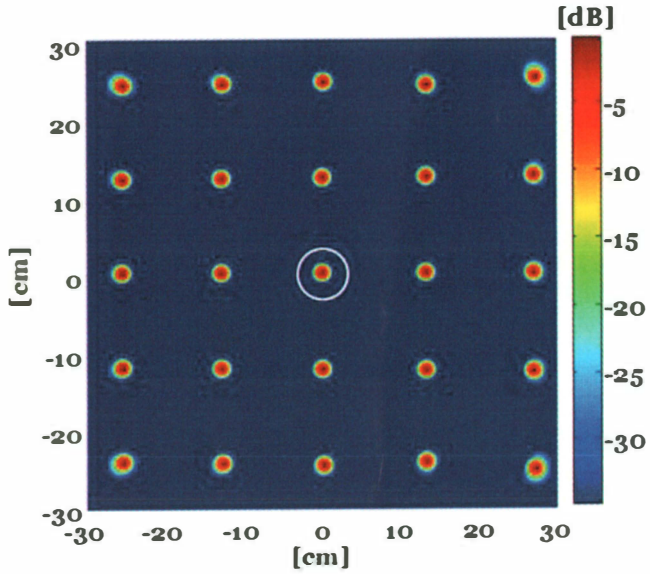

Figure 5a. A physical-optics simulation of the imager beam patterns, assuming a point target and identical transmitted/received beam shapes.

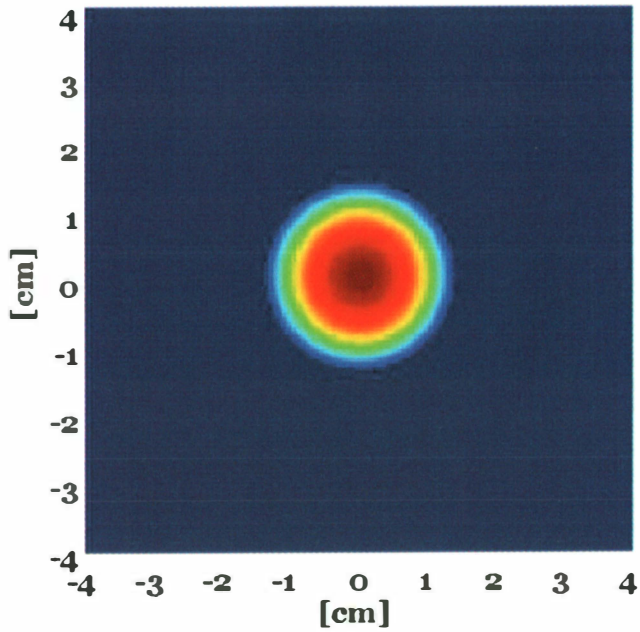

Figure 5b. An expanded view of the central pattern from Figure 5a. The same color scale applies for both figures.

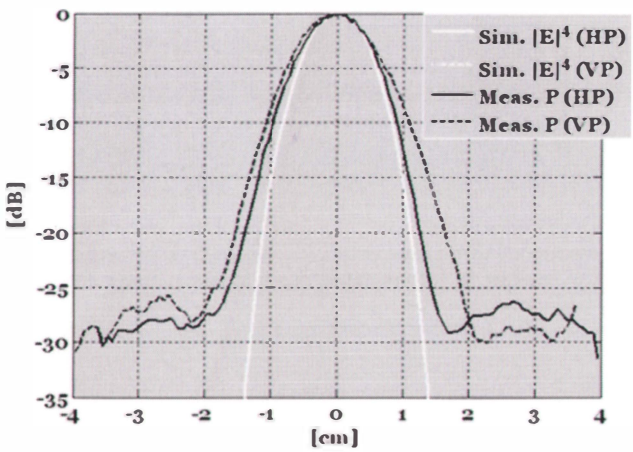

Figure 6a. The simulated and measured patterns are compared along the main cuts for the central beam outlined in Figure 3b. HP and VP stand for horizontal and vertical plane, respectively.

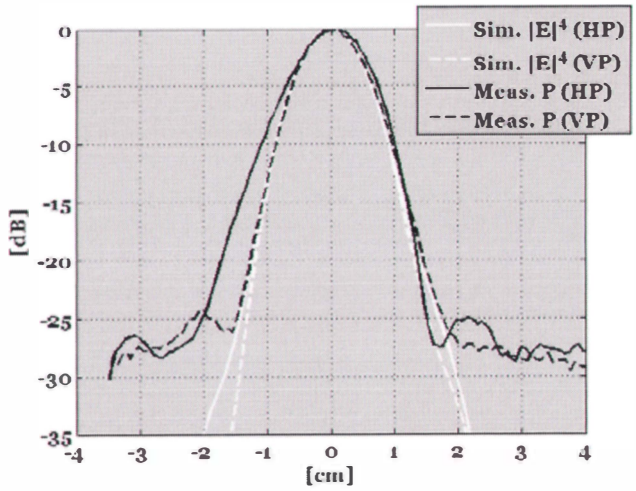

Figure 6b. The simulated and measured patterns are compared along the main cuts for the edge beam outlined in Figure 3b. HP and VP stand for horizontal and vertical plane, respectively.

Figure 5a shows the squared power, $P^2 \sim |E|^4$, of the simulated scanned antenna patterns, corresponding to the 5 × 5 grid of targets as in Figure 3. These patterns were simulated with the commercial software *GRASP* from TICRA. The squared power is used for comparison because the received power of the radar was proportional to the product of the transmitted and received antenna patterns, which we assumed to be the same. The patterns shown in Figure 5a corresponded to the same directions as the target grid shown in Figure 3a. A closer view of the central pattern is shown in Figure 5b. These simulated patterns did not take into account the finite width of the 3 mm beads in Figure 3; rather, they assumed an infinitesimal point reflector. The simulated and measured patterns in the main cuts are compared in Figure 6 for the central beam and the right-upper-corner beam (as marked in Figure 3b). The comparison between the simulations and measurements was very good, considering the limited alignment tolerances at this high frequency, the mirror-surface tolerances, the fact that measurements were performed with targets of finite-sized targets, and any scattering effects from the suspending nylon threads. The measurement dynamic range of around 25-30 dB was thermal-noise limited, set by the system's noise temperature and the single-pixel integration time of 0.44 ms. The half-power beamwidths of the measured beams exceeded the simulated half-power beamwidths by an average of only about 9%. This was less than the ratio of the target sphere's diameter and the half-power beamwidth (i.e., 23%). It is important to point out that the measurement method itself was not accurate enough to provide a better assessment of the half-power beamwidth because of the finite sphere diameter, a limited SNR, and the few-cm uncertainty in the actual target distance. However, the main discrepancies with the simulations likely came from the fabrication tolerances (the antenna surfaces were not tested after

being fabricated) and misalignments. The beam shapes reported here were obtained with only a small effort for beam alignment, consisting of adjustments made by hand to the antenna system's elements while observing the scan of Figure 3 evolve in real time.

3. Imaging Performance

A THz radar image was acquired by raster scanning the radar beam across the field of view, as shown in Figure 7a. The yellow dot represents the antenna beam at the nominal position of the rotating mirror, i.e., the central beam in Figures 3 and 5. The red lines show the serpentine scan path, with the elevation and azimuth being the fast and slow directions, respectively. The vertical scanning was accomplished with a fast precision rotator that accelerated for the first half of the scan, e.g., from –3° to 0°, and then decelerated for the second half, e.g., from 0° to +3°. (This was a "bang-bang" control approach to achieve a scan time limited by maximum motor torque.) With a constant acceleration magnitude a, the acquisition time for a single vertical line is $T_v = 2\sqrt{\frac{D_v}{a}}$, where D_v is the number of degrees spanned in the vertical direction for the mirror rotation (i.e., θ_m). The number of horizontal and vertical pixels is then typically chosen to have a spacing that is half of the two-way beamwidth ($HPBW_2$) to maintain good image quality, which gives a spacing of about 0.5 cm for the system described here. The numbers of horizontal and vertical pixels are thus $N_h = N_v = \frac{D_v}{HPBW_2/2}$ for a square scan area with equal horizontal and vertical spans, $D_h = D_v$. From these parameters, the total image-acquisition time can be expressed as $T = N_h T_v = N_h 2\sqrt{\frac{D_v}{a}}$, with the horizontal motor rotation speed kept constant at $v_h = \frac{D_h}{T}$.

With a uniform pixel spacing and a constant nodding-mirror acceleration magnitude, the dwell time per pixel must be shorter than $t_d \le \frac{T_v}{2N_v} = \frac{1}{N_v}\sqrt{\frac{D_v}{a}}$. For a span angle of 6°, a 100 × 100 pixel image, and an acceleration of 20,000°/s^2, this implies a maximum dwell time of 0.17 ms (and a total image time of 3.5 s). However, unfortunately the radar's pulse repetition interval is currently limited by the minimum chirp time of the DDS/PLL hybrid chirp-synthesizer architecture, which is around $t_d = 0.5$ ms. This constitutes the present imaging-speed bottleneck, although an order-of-magnitude improvement will be achieved soon from a chirper redesign. The maximum useful mirror acceleration is thus around 2,400°/s^2 for a minimum 100 × 100 pixel image time of about 10 seconds.

Figure 8 shows an example of concealed-weapon detection at a 25 m standoff range, performed with the presented antenna system, and using the back-surface radar-imaging processing technique described in [5]. The threat in this case was a metal handgun (Figure 8a), concealed by a fleece jacket. The THz radar image is shown in Figure 8b, superimposed on the optical image. The image spanned about 38 × 38 cm (i.e. $D_h = D_v \approx 4.6°$) with $N_h = N_v = 69$, yielding an acquisition time of about five seconds. The single-pixel dwell time for this image was 0.5 ms, and the fast-rotating mirror's acceleration magnitude was 3,600°/s^2.

The five-second imaging time for Figure 8 was limited by the chirp time, and it is unacceptably long for most real-world applications. Somewhat higher imaging speeds can be achieved with a faster chirp source and a faster rotating motor. However, as discussed in [16], an important limiting factor for the speed is set by the SNR level of the radar. Because of the coherent-detection technique, the SNR of a single-pixel acquisition is proportional to the signal-integration time, i.e., the waveform-chirp duration. The individual radar spectra from the dataset in Figure 8b exhibited SNRs spanning about 25-45 dB, and the imaging speed can likely be increased by 10 dB (to 0.5 s) without being SNR limited [16]. The current system thus might be able to attain 2 Hz frame rates without any need for higher-power THz sources or source arrays.

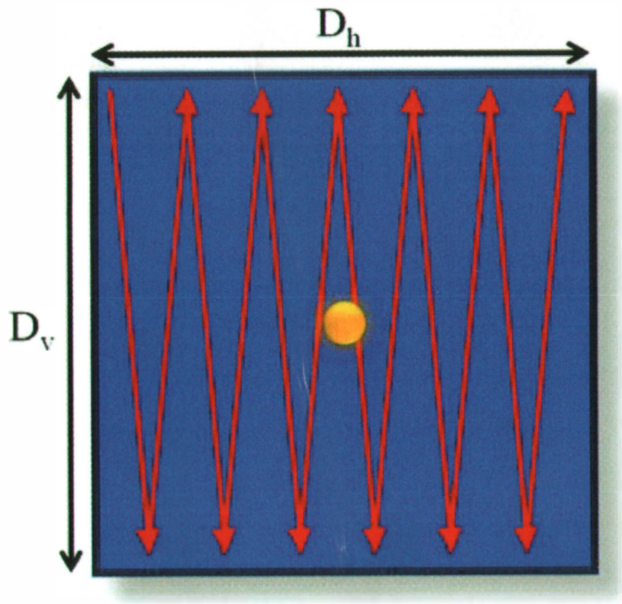

Figure 7a. A drawing showing the imager raster scan using a single pixel. The horizontal and vertical dimensions are related to the mirror-rotation angles.

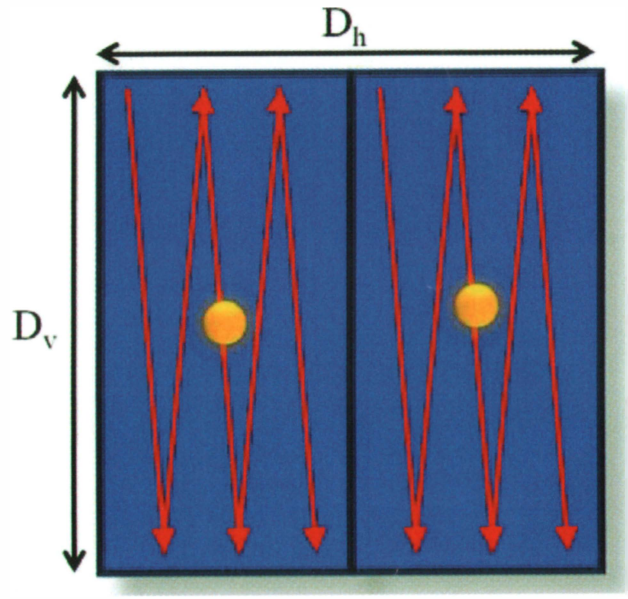

Figure 7b. A drawing showing the imager raster scan using two simultaneous pixels. The horizontal and vertical dimensions are related to the mirror-rotation angles.

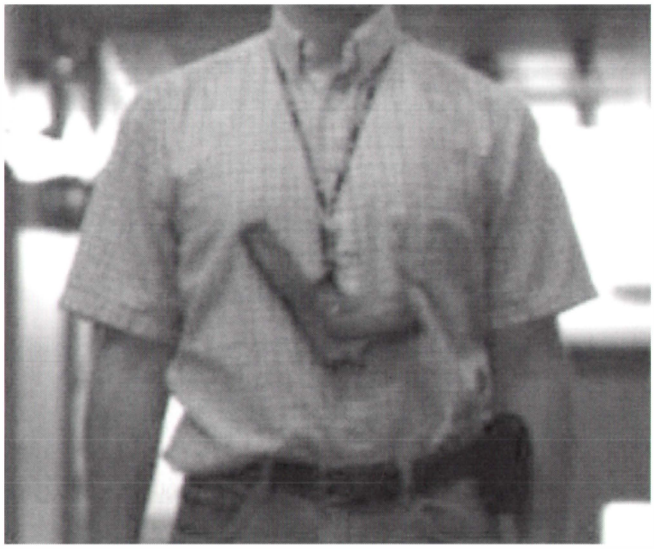

Figure 8a. A person wearing a handgun around his neck at 25 m standoff range with no jacket.

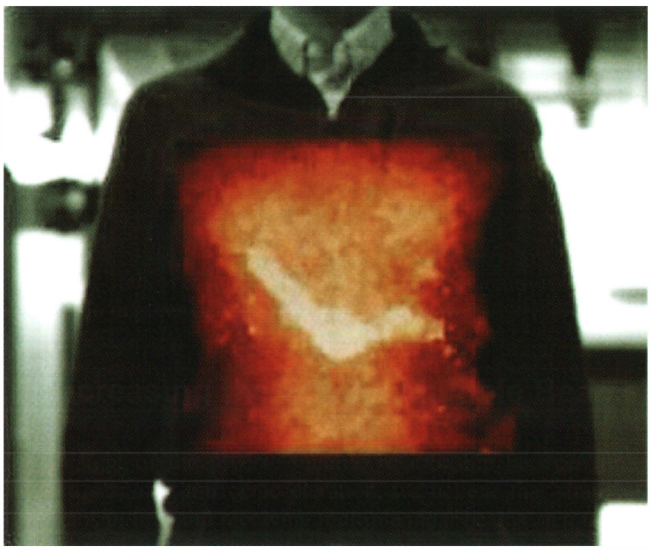

Figure 8b. When covered with a fleece jacket, the handgun from Figure 8a was detected in five seconds using the fast-scanning THz imaging radar.

However, implementing a robust scanning motor capable of covering 6° × 6° with precisely spaced pixels at a 100 × 100 density is far from a trivial exercise. For example, because of the square-law relationship, the flat-mirror acceleration and the imaging time, $a \sim T^{-2}$, extending the a fast-rotating flat-mirror speed to reach a 2 Hz frame rate over a 6° span will require accelerations of nearly one million degrees per second squared!

4. Increasing the Speed: Multiple Beams

In light of the inverse-squared relationship between image time and scanning-mirror acceleration, we believe that simultaneously transmitting and receiving multiple radar beams on a target is the only realistic path toward near-video-rate THz-radar imaging. To simultaneously project several beams onto the target using the same antenna system presented here, a small array of transceivers could be placed in the focal plane of the feed reflector, as depicted in Figure 9. There is a substantial difference in acquisition time, depending on whether the array lies in the vertical or horizontal direction, for the antenna system described here:

- Horizontal linear array ($N_a \times 1$): the positions of the array will be chosen such that their beams are equidistantly distributed across the field of view. The effective number of horizontal pixels will be N_h/N_a. This implies that the total time will be also reduced by N_a, whereas the horizontal motor speed will be kept the same.

- Vertical linear array ($1 \times N_a$): The vertical-scan distance is now reduced to D_y/N_a. However, the total time will only be reduced by $\sqrt{N_a}$, because of the square-root dependence of T_v on D_y.

It is therefore preferable to have a linear array in the horizontal plane, assuming fast scanning in the vertical plane. From the antenna point of view, a horizontal array is also more convenient, because the reflector's surfaces are offset with respect to their symmetry axis in the vertical plane, which would imply higher distortions for off-focus feed in the vertical plane than in the horizontal plane. As a concrete example, if an eight-beam array were used (horizontally), with a vertical fast-scanning mirror acceleration of 20,000°/s², the 3.5 s image time would be divided by eight, to reach very practical >2 Hz frame rates for the full 6° × 6° scan. Alternatively, if a smaller 4.6° × 4.6° field of view were acceptable as in Figure 6, then an additional ~50% frame-rate improvement is possible.

The scanning associated with the array is done subsequently to the beams leaving the feed reflector. For example, consider the case when the mirror is at its nominal position. A spatial displace-

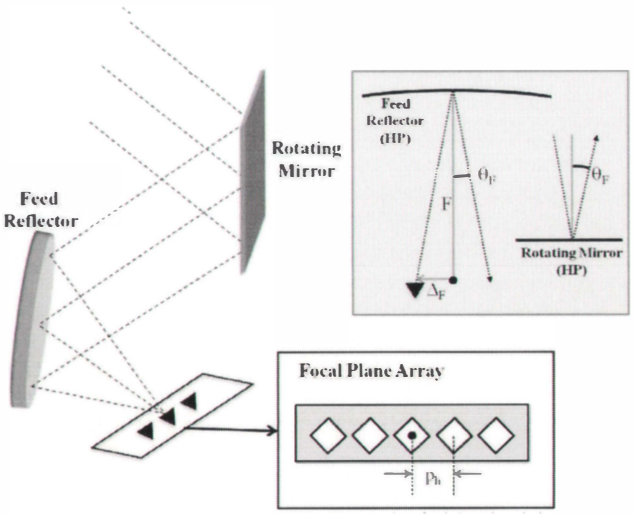

Figure 9. The concept of a linear array of transceivers placed in the THz radar's focal plane along the horizontal axis of the feed-reflector. The array elements are placed at period p_h, as shown in the lower-right inset. In the upper-right inset, the scanning mechanism is shown: a feed displacement of Δ_F will tilt the feed-reflector beam by θ_F, and that beam will intersect the rotating mirror at an angle θ_F, leading to $\theta_{sm} = \theta_F$.

ment of Δ_F along the horizontal axis of the feed reflector scans the beam towards $\theta_F = \frac{\Delta_F}{F} BDF_F$, where F and BDF_F are the focal distance and beam-deviation factor of the feed reflector, respectively. The angle of the beam after the mirror will be $\theta_{sm} = \theta_F$, which will scan the antenna beam as described in Section 2 (see Figure 2).

The array elements are placed at distances of Δ_F, chosen to have D_h/N_a. For example, if we want to have a 2 × 1 array, the beams intersecting the mirror diverge by 6° (i.e., $\theta_{sm} = \pm 3°$), and the raster scan of Figure 7b would apply. To obtain such separation in the current antenna system, where $F = 223.7$ mm, and considering $BDF_F = 1$, the feeds are placed at $\Delta_F = \pm 11.7$ mm. This configuration was simulated with *GRASP*, and the results are shown in Figure 10. Figure 10a shows the far-field patterns of the feed reflector, showing a beam separation of 5.93°. Figure 10b shows the down-range patterns of the whole antenna system, where the beams point towards $\Delta_s = 12.97$ cm.

The patterns presented in Figure 10 suffer from some distortions that create an elliptical shape. These distortions were already present in the collimated beam formed between the feed reflector and the rotating mirror (see Figure 7a). This is because they are associated with the poor off-focus feed performance of an offset reflector [17], which in this case is the feed reflector. Such distortions could be significantly reduced by replacing the current parabolic feed reflector by an optimized dual-reflector system [18].
In general, the elements of the $N_a \times 1$ are placed at a period of $p_h = \frac{F}{BDF_F} \frac{2D_h}{N_a}$, with D_h given in radians. For the 2×1 array, the horns are separated by 23.4 mm. This separation is very convenient, because many sub-millimeter-wave components (horns, mixers, multipliers) are made in aluminum blocks of approximately this dimension. For a larger number of elements with a closer packing, the fabrication of heterodyne arrays becomes a challenge at these high frequencies, and advanced integration techniques are needed [19].

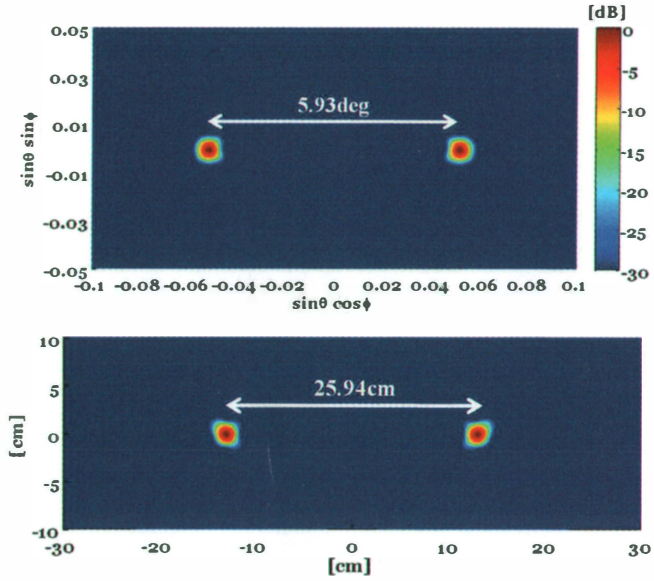

Figure 10. A physical-optics simulation of (a) the feed-reflector far-field pattern and (b) the imager pattern ($|E|^4$) at 25 m, for a 2 × 1 array of transceivers with the elements placed at $\Delta_F = \pm 11.7$ mm from the focus of the feed reflector, as described in Figure 9.

4.1 Time-Delay Multiplexing

Instead of duplicating the transceiver to achieve multiple beams, as described above, we can use the time-multiplexing technique introduced in [10]. This technique consists of generating a second beam with the power lost from the beam splitter by using a quasi-optical waveguide to introduce a time delay with respect to the original beam. Both the original and the time-delayed beams are detected using the same receiver port. Their signals can be distinguished as a shift in the FMCW radar's down-converted frequency spectrum, because the time delay is much greater than the radar's resolution and the range span of a typical human target's surface.

We modified the time-delay multiplexing design of [10] to fit in the current 25 m antenna system, and a geometrical description is shown in Figure 11. This multiplexing approach used orthogonal polarizations of the two beams, along with wire grids, to separate and combine them without losing any significant power. The orange line represents the beam path of the main beam (the horn was placed at $\Delta_F = 11.7$ mm, as described in the previous section for the 2×1 array). The blue line shows the beam path of the beam that is delayed through the quasi-optical waveguide. This delay

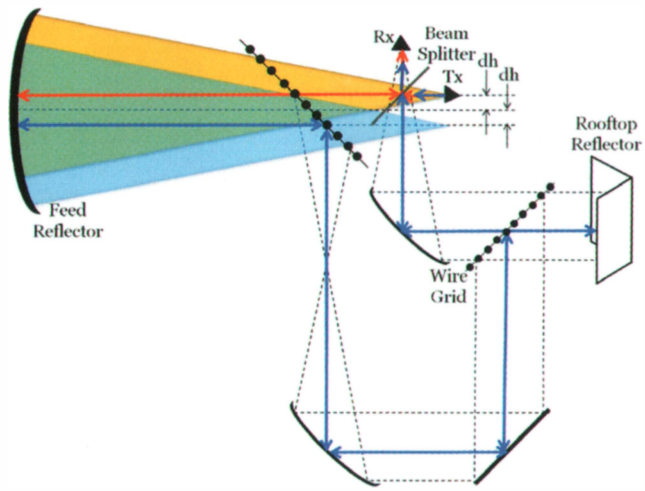

Figure 11. The geometry of the quasi-optical waveguide used for time multiplexing of a second pixel from a single transceiver.

path consisted of two parabolic reflectors to collimate the beam, a rooftop reflector to rotate the polarization, and two wire grids to manipulate the cross-polarized beams. The quasi-optical waveguide was designed so that the virtual focus of the second beam was at $\Delta_F = -11.7$ mm in the focal plane of the feed reflector, as indicated by the blue cone in the figure, giving rise to a second beam, as in the 2×1 array. This system was also simulated with *GRASP*, and the beams obtained were basically the same as those shown in Figure 10b. This configuration will allow using the raster scan of Figure 7b. It therefore can double the speed without increasing the number of transceivers or the complexity of the radar back-end hardware. The same concept can be applied to double the number of beams of a linear array, as described in [10].

5. Conclusion

At present, there is growing interest in using THz imaging systems to detect concealed weapons under clothes at long standoff ranges. The systems need to be fast and have very good beam quality, in order to be feasible for realistic threat situations. In this contribution, we have presented a practical implementation of an antenna system that can achieve fast imaging at long range. The proposed antenna system utilizes a Gregorian confocal reflector geometry, with a small mechanical rotating mirror that allows steering the beam without sacrificing beam quality. The system has been fabricated and tested successfully. We have shown THz imagery of targets at 25 m standoff ranges being obtained in five seconds. The next step is to achieve frame rates exceeding 2 Hz, which is feasible with the use of a heterodyne THz array of just a few elements (two or four). Alternatively, the array can be designed in combination with time-delay multiplexing techniques that allow doubling the number of beams, while still using only a single transceiver.

6. Acknowledgments

Part of this research was carried out at the Jet Propulsion Laboratory, California Institute of Technology, under a contract with the National Aeronautics and Space Administration. We gratefully acknowledge the support of the Naval Explosive Ordnance Disposal Technology Division with funding provided by the Department of Defense (DoD) Physical Security Equipment Action Group (PSEAG). N. Llombart is currently contracted by the Universidad Complutense de Madrid under the "Ramón y Cajal" research program of the Spanish Ministry of Science and Innovation.

7. References

1. R. Appleby and H. B. Wallace, "Standoff Detection of Weapons and Contraband in the 100 GHz to 1 THz Region," *IEEE Transactions on Antennas and Propagation*, **AP-55**, 11, November, 2007, pp. 2944-2956.

2. H. B. Liu, Y. Chen, G. J. Bastiaans, and X.-C. Zhang, "Detection and Identification of Explosive RDX by THz Reflection Spectroscopy," *Optics Express*, **14**, 2006, pp. 415-423.

3. For example, see Thruvision Systems Ltd., Brijot Imaging Systems Inc., Sago Systems Inc., and Millivision Corp.

4. A. Luukanen, P. Helistö, P. Lappalainen, M. Leivo, A. Rautiainen, H. Toivanen, H. Seppä, Z. Taylor, C. R. Dietlein, and E. N. Grossman, "Stand-Off Passive THz Imaging at 8-Meter Stand-Off Distance: Results from a 64-Channel Real-Time Imager," Proceedings of SPIE **7309**, 73090F, 2009.

5. K. B. Cooper, R. J. Dengler, N. Llombart, T. Bryllert, G. Chattopadhyay, E. Schlecht, J. Gill, C. Lee, A. Skalare, I. Mehdi, and P. H. Siegel, "Penetrating 3D Imaging at 4 and 25 Meter Range Using a Submillimeter-Wave Radar," *IEEE Transactions on Microwave Theory and Techniques*, **56**, 12, December, 2008, pp. 2771-2778.

6. C. am Weg, W. von Spiegel, R. Henneberger, R. Zimmermann, T. Loeffler, and H. G. Roskos, "Fast Active THz Cameras with Ranging Capabilities," *Journal of Infrared, Millimeter, and Terahertz Waves*, **30**, 12, 2009, pp. 1281-1296.

7. D. M. Sheen, T. E. Hall, R. H. Severtsen, D. L. McMakin, B. K. Hatchell, and P. L. J. Valdez, "Active Wideband 350GHz Imaging System for Concealed-Weapon Detection," Proceedings of the SPIE, **7309**, 2009.

8. R. J. Dengler, K. B. Cooper, N. Llombart, G. Chattopadhyay, T. Bryllert, I. Mehdi, and P. H. Siegel, "Toward Real-time Penetrating Imaging Radar at 670 GHz," 2009 IEEE MTT-S Intl. Microwave Symposium Digest, 2009, pp. 941-944.

9. N. Llombart, K. B. Cooper, R. J. Dengler, T. Bryllert, and P. H. Siegel, "Confocal Ellipsoidal Reflector System for a Mechanically Scanned Active Terahertz Imager," *IEEE Transactions on Antennas and Propagation*, **AP-58**, 6, June 2010, pp. 1834-1841.

10. N. Llombart, K. B. Cooper, R. J. Dengler, T. Bryllert, G. Chattopadhyay, and P. H. Siegel, "Time Delay Multiplexing of Two Beams in a THz Imaging Radar," *IEEE Transactions on Microwave Theory and Technology*, **58**, 8, August, 2010.

11. J. A. Martinez-Lorenzo, A. Garcia-Pino, B. Gonzalez-Valdes, and C. M. Rappaport, "Zooming and Scanning Gregorian Confocal Dual Reflector Antennas," *IEEE Transactions on Antennas and Propagation*, **AP-56**, 9, September, 2008, pp. 2910-2919.

12. A. W. Rudge, K. Milne, A. Olver, and P. Knight, *The Handbook of Antenna Design*, London, UK, Peter Peregrinus, 1986.

13. R. I. Hunter, D. A. Robertson, P. Goy, and G. M. Smith, "Design of High-Performance Millimeter Wave and Sub-Millimeter Wave Quasi-Optical Isolators and Circulators," *IEEE Transactions on Microwave Theory and Technology*, **55**, 5, May, 2007, pp. 890-898.

14. J. F. Johansson and N. D. Whyborn, "The Diagonal Horn as a Sub-Millimeter Wave Antenna," *IEEE Transactions on Microwave Theory and Technology*, **40**, 5, May, 1992, pp.795-800.

15. J. Ruze, "Antenna Tolerance Theory – A Review," *Proceedings of the IEEE*, **54**, 4, April 1966, pp. 633-640.

16. K. B. Cooper, R. J. Dengler, N. Llombart, A. Talukdera, A. V. Panangadana, C. S. Peaya, and P. H. Siegel, "Fast, High-Resolution Terahertz Radar Imaging at 25 Meters," Proceedings of the SPIE, **7671**, 2010.

17. Y. Rahmat-Samii, "Reflector Antennas," in Y. T. Lo and S. W. Lee (eds.), *Antenna Handbook*, New York, Van Nostrand Reinhold, 1988.

18. W. V. T. Rusch, A. Prata, Y. Rahmat-Samii, and R. A. Shore, "Derivation and Application of Equivalent Paraboloid for Classical Offset Cassegrain and Gregorian Antennas," *IEEE Transactions on Antennas and Propagation*, **AP-38**, 8, August 1990, pp. 1141-1149.

19. I. Mehdi, B. Thomas, C. Lee, G. Chattopadhyay, R. Lin, E. Schlecht, A. Peralta, J. Gill, K. B. Cooper, N. Llombart, and P. H. Siegel, "Radiometer-on-a-Chip: A Path Towards Super-Compact Submillimeter-Wave Imaging Arrays," Proceedings of the SPIE, **7671**, 2010.